Correction

NEUROSCIENCE

Correction for "Genome-wide screen identifies curli amyloid fibril as a bacterial component promoting host neurodegeneration," by Chenyin Wang, Chun Yin Lau, Fuqiang Ma, and Chaogu Zheng, which published August 19, 2021; 10.1073/pnas.2106504118 (*Proc. Natl. Acad. Sci. U.S.A.* **118**, e2106504118).

The authors note that two references were omitted from the article. The complete references appear below. A citation to the first new reference (42) should be included on page 11, left column, first paragraph, line 12, after "...thus promote neurodegeneration." To incorporate the second new reference, the sentence beginning "While we were conducting this study..." (page 11, left column, second paragraph, line 14) should be extended by adding ", which supported an earlier finding that curli enhanced α-syn deposition in the brain of aged rats (44)." The original ref. 42 (Sampson et al.) should be renumbered as ref. 43. The phrase "their in vitro studies" in the following sentence on page 11, left column, second paragraph, line 17, should be replaced by "these studies" to make the sentence more coherent.

The authors also want to add the acknowledgement of Tingying Xia, Aixin Yan, and Patrick C. Y. Woo for their efforts in providing the *E. coli* UTI2 strain: "We thank Tingying Xia and Aixin Yan (School of Biological Sciences, The University of Hong Kong) and Patrick C. Y. Woo (Department of Microbiology, Li Ka Shing Faculty of Medicine, The University of Hong Kong) for providing the *E. coli* UTI2 strain, which was isolated at Queen Mary Hospital, Hong Kong."

The online version has been corrected.

42. R. P. Friedland, Mechanisms of molecular mimicry involving the microbiota in neurodegeneration. *J. Alzheimers Dis.* **45**, 349–362 (2015).
43. T. R. Sampson *et al.*, A gut bacterial amyloid promotes α-synuclein aggregation and motor impairment in mice. *eLife* **9**, e53111 (2020).
44. S. G. Chen *et al.*, Exposure to the functional bacterial amyloid protein curli enhances alpha-synuclein aggregation in aged fischer 344 rats and *Caenorhabditis elegans*. *Sci. Rep.* **6**, 34477 (2016).

Published October 8, 2021.

www.pnas.org/cgi/doi/10.1073/pnas.2116257118

Genome-wide screen identifies curli amyloid fibril as a bacterial component promoting host neurodegeneration

Chenyin Wang (汪辰吟)[a], Chun Yin Lau[a], Fuqiang Ma[a], and Chaogu Zheng (郑超固)[a,1]

[a]School of Biological Sciences, The University of Hong Kong, Hong Kong Special Administrative Region, China

Edited by Gary Ruvkun, Massachusetts General Hospital, Boston, MA, and approved July 1, 2021 (received for review April 7, 2021)

Growing evidence indicates that gut microbiota play a critical role in regulating the progression of neurodegenerative diseases such as Parkinson's disease. The molecular mechanism underlying such microbe–host interaction is unclear. In this study, by feeding *Caenorhabditis elegans* expressing human α-syn with *Escherichia coli* knockout mutants, we conducted a genome-wide screen to identify bacterial genes that promote host neurodegeneration. The screen yielded 38 genes that fall into several genetic pathways including curli formation, lipopolysaccharide assembly, and adenosylcobalamin synthesis among others. We then focused on the curli amyloid fibril and found that genetically deleting or pharmacologically inhibiting the curli major subunit CsgA in *E. coli* reduced α-syn–induced neuronal death, restored mitochondrial health, and improved neuronal functions. CsgA secreted by the bacteria colocalized with α-syn inside neurons and promoted α-syn aggregation through cross-seeding. Similarly, curli also promoted neurodegeneration in *C. elegans* models of Alzheimer's disease, amyotrophic lateral sclerosis, and Huntington's disease and in human neuroblastoma cells.

Parkinson's disease | curli | neurodegeneration | microbe–host interaction

Neurodegenerative diseases are characterized by protein misfolding and aggregation, leading to the formation of amyloid fibril enriched in β-sheet structures. Such protein aggregates trigger proteotoxicity, overwhelm the chaperone and degradation machineries, and eventually cause neuronal death (1). For example, Parkinson's disease (PD) is associated with the intracellular aggregation of α-synuclein (α-syn) into Lewy bodies and Lewy neurites, which causes the degeneration of mostly dopaminergic (DA) neurons in the substantia nigra (2). The loss of DA neurons leads to decreased dopamine signaling in the striatum, which results in impaired motor functions in PD patients. α-syn is a small (140–amino acid) protein made of an N-terminal domain, a non–A-β component domain that is the fibrilization core, and a carboxyl-terminal region. Missense mutations in the N-terminal domain, such as A30P, G46K, and A53T, result in autosomal dominant familial PD by producing mutant proteins that are more prone to misfolding and aggregation than the wild-type proteins (3). Mutant α-syn proteins form toxic β-sheet–like oligomers that cause mitochondrial dysfunctions, oxidative stress, disruption in calcium homeostasis, and neuroinflammation, which all lead to neurodegeneration (2). Effective therapeutic intervention that prevents α-syn aggregation is currently missing.

Studies in the last few years have suggested that the gut microbiota may play an important role in the pathogenesis of neurodegenerative diseases (4). For example, antibiotic treatment ameliorates the pathophysiology of PD mice, and microbial recolonization after the treatment restored the PD symptoms (5). Colonization of α-syn–overexpressing mice with microbiota from PD patients exacerbated the physical impairments compared to transplantation of microbiota from healthy donors (5). In addition to animal models, clinical studies have also provided evidence for a microbiota–gut–brain link in PD. Gastrointestinal dysfunction was frequently found in PD patients (6), and infection with *Helicobacter pylori* has been linked with disease severity and progression (7). Sequencing of the fecal samples of PD patients revealed changes in the gut bacterial composition (e.g., increased *Lactobacillaceae*) compared to healthy individuals (8, 9). Similar to PD, gut bacteria in mouse models of Alzheimer's disease (AD) promoted amyloid pathology (10), and altered gut microbiome composition was also observed in AD patients (11).

Despite the growing connection between the disturbed gut microbiota and the development of neurodegenerative diseases, mechanistic understanding of the communication between the bacteria and the nervous system is limited. Most theories focus on the neurodegenerative effects of the systemic inflammation and neuroinflammation caused by the abnormal microbiota. Whether bacteria proteins or metabolites can directly act on the host neurons to module the progression of neurodegeneration induced by α-syn or A-β proteotoxicity is unclear. This limitation is largely due to the lack of a simple model that allows systematic tests of individual bacterial components for their neuronal effects.

To address the problem, we employed a *Caenorhabditis elegans* model of PD that expressed the human α-syn proteins in *C. elegans* neurons to investigate the mechanisms of microbial regulation on PD. Because *C. elegans* uses bacteria as its natural diet and can be easily cultivated under monoaxenic conditions, it has emerged as an important organism to model microbe–host interaction. In fact, alteration of the bacterial genome affected the development, metabolism, and behavior of *C. elegans* (12, 13). Several studies

Significance

We investigate microbe–host interaction in the context of neurodegeneration by screening for *Escherichia coli* genes whose deletion alleviates Parkinson's disease symptoms in the nematode *Caenorhabditis elegans* overexpressing human α-synuclein (α-syn, A53T). The screen yields 38 *E. coli* genes that promote neurodegeneration. Two of these genes, *csgA* and *csgB*, code for proteins that form curli, one type of bacterial amyloid fibers. Curli cross-seeds and colocalizes with α-syn both in *C. elegans* neurons and human neuroblastoma cells. Curli-induced α-syn aggregations down-regulate mitochondrial genes, causing energy failure in neurons. Moreover, we found that curli may have general effects in promoting neuropathologies induced by different aggregation-prone proteins, such as A-β in Alzheimer's disease, Huntingtin in Huntington's disease, and SOD1 in amyotrophic lateral sclerosis.

Author contributions: C.W. and C.Z. designed research; C.W. performed research; C.W., C.Y.L., F.M., and C.Z. analyzed data; and C.W. and C.Z. wrote the paper.

The authors declare no competing interest.

This article is a PNAS Direct Submission.

[1]To whom correspondence may be addressed. Email: cgzheng@hku.hk.

This article contains supporting information online at https://www.pnas.org/lookup/suppl/doi:10.1073/pnas.2106504118/-/DCSupplemental.

Published August 19, 2021.

also showed that certain bacterial metabolites could influence neurodegeneration in *C. elegans* (14–16).

In this study, we screened all nonessential *Escherichia coli* genes for their effects on PD pathogenesis by feeding individual *E. coli* knockout mutants to PD *C. elegans* and assessing the severity of neurodegeneration. This screen identified 38 *E. coli* genes whose deletion led to amelioration of PD symptoms. These genes fall into distinct genetic pathways including curli formation, lipopolysaccharide (LPS) production, lysozyme inhibition, adenosylcobalamin synthesis, and oxidative stress response, suggesting that diverse bacteria components could promote neurodegeneration. As an example, we focused on the role of bacterial curli amyloid fibril on PD and found that deleting the curli genes *csgA* and *csgB* in the *E. coli* genome reduced α-syn–induced cell death, restored mitochondrial health, and improved neuronal functions. Using antibody staining and biochemical analysis, we showed that CsgA promoted α-syn aggregation and that removing curli in the bacteria diet enabled proteasome-dependent degradation of α-syn. Importantly, we demonstrated in vivo colocalization and cross-seeding between bacteria-derived CsgA and α-syn in dopaminergic neurons; this cross-seeding significantly enhanced α-syn aggregation. Moreover, we extended our findings into *C. elegans* models of AD, amyotrophic lateral sclerosis (ALS), and Huntington's disease (HD) and into human neuroblastoma SH-SY5Y cells. Overall, our studies indicate that bacterial components, such as curli, can have direct neurodegenerative effects.

Results

A Genome-Wide Screen Identified *E. coli* Genes that Promote Human α-synuclein–Induced Neurodegeneration in *C. elegans*. To systematically identify bacterial genes that contribute to neurodegeneration in the host, we employed *C. elegans* transgenic animals that express the human α-syn in all neurons and screened for *E. coli* K12 knockout mutants that could ameliorate *C. elegans* neurodegenerative phenotypes when fed to the animals. Pan-neuronal expression (using the *aex-3* promoter) of the proaggregating human α-syn A53T mutants, but not the wild-type α-syn, led to degeneration of the motor neurons, causing uncoordinated (Unc) movements in both larva and adults (17). The penetrance of this Unc phenotype is 100% in animals carrying the *aex-3p::α-syn(A53T)* transgene and fed with the wild-type *E. coli* K12 strain. By screening the 3,985 K12 knockout mutants in the Keio collection (18), we identified 380 *E. coli* mutants that restored normal locomotion (non-Unc) in at least 25% of the PD animals in the first round (Fig. 1*A*). These 380 positive clones were subjected to three more rounds of locomotion screens, and we obtained 172 mutants that led to consistent recovery of locomotion in ≥25% of the PD animals on average (Fig. 1*B*). We then subjected the 172 positive clones to a visual screen for the suppression of neuronal death using a DA neuronal marker. When fed with wild-type K12, only ∼10% of the PD animals carrying the *aex-3p::α-syn(A53T)* transgene had two visible ADE neurons labeled by *dat-1p::GFP* at day 2 adult stage (Fig. 1*C*). By screening the 172 clones for three repeated rounds, we identified 104 *E. coli* mutants that resulted in the survival of two ADE neurons in ≥25% of the animals on average.

To avoid any bias associated with specific genetic background, we conducted a separate visual screen using an independent PD model, in which the human α-syn A53T mutant protein was expressed from the DA-specific *dat-1* promoter. We fed the 380 first-round positive *E. coli* knockout mutants to animals carrying the *dat-1p::α-syn(A53T)* transgene. Through three rounds of screens, we identified 78 *E. coli* mutants that led to the survival of two ADE neurons in ≥25% of the animals in the DA-specific degenerative model (Fig. 1*A*). By overlapping these 78 positive clones with the 104 positive hits found using the pan-neuronal model, we obtained the final 38 *E. coli* mutants that significantly inhibited neurodegeneration induced by human α-syn A53T mutants.

We categorized the 38 *E. coli* genes that contribute to neurodegeneration based on their functions, and several microbial genetic pathways emerged (Table 1). For example, we identified genes responsible for the formation of curli amyloid fibril (*csgA* and *csgB*), the production and assembly of LPS (*lapA*, *lapB*, *lpcA*, *rfe*, and *pldA*), the salvage pathway–dependent synthesis of vitamin B12 adenosylcobalamin (*cobS*, *btuR*, and *eutT*), the inhibition of eukaryotic lysozyme (*ivy* and *ydhA*), as well as genes involved in oxidative stress response, energy homeostasis, membrane transport, and other functions. Our systematic screen revealed extensive microbe–host interactions, through which bacterial molecules promote α-syn proteotoxicity and neurodegeneration in the host. In this study, we focus on the mechanisms by which bacterial curli promotes neurodegeneration.

Curli Subunits CsgA and CsgB Are Required for α-syn–Induced Degenerative Phenotypes. Among the top hits in our screen are *csgA* and *csgB*, which code for the major and minor curli subunits, respectively. Curli are amyloid fibril secreted by certain enterobacterial strains, such as *E. coli* and *Salmonella*, and are important for biofilm formation (19). Deletion of *csgA* or *csgB* in *E. coli* K12 fed to *C. elegans* resulted in significantly improved motor functions (measured as the number of body bends per 20 s) in animals expressing α-syn(A53T) pan-neuronally (Fig. 1*D*) and largely restored DA neuron functions (measured as food-induced basal slowing response) in animals expressing α-syn(A53T) specifically in DA neurons (Fig. 1*E*). These results suggest that *E. coli* curli promotes α-syn–induced neurodegeneration in *C. elegans*.

Congo red can stain curli amyloid fibril. As expected, deletion of *csgA* and *csgB* led to the complete loss of Congo red staining (Fig. 2*A*). We also stained the other 36 *E. coli* mutants identified from our screen and found that *tolQ(-)*, *lpcA(-)*, *lapA(-)*, and *lapB(-)* mutants showed weak Congo red staining, indicating reduced curli production. These four genes were previously found to be associated with curli biogenesis (20), so their effects in promoting neurodegeneration may be partly connected to their roles in enhancing curli production. In contrast, the remaining 32 mutants showed largely wild-type level of staining (*SI Appendix*, Fig. S1*A*).

To support that curli functions as structured protein fibrils in *C. elegans*, we heat-killed the K12 wild-type bacteria to denature all proteins and found that the heat kill phenocopied the *csgA(-)* and *csgB(-)* deletion in suppressing α-syn–induced locomotion defects and ADE degeneration (Fig. 2*B*). Importantly, heat kill did not further enhance the effects of curli deletion. Interestingly, mixing the wild-type K12 with *csgA(-)* or *csgB(-)* bacteria strongly suppressed the neuroprotective effects of the mutants, suggesting that a small amount of curli may be enough to trigger neurodegeneration (Fig. 2*B*). Moreover, mixing *csgA(-)* with *csgB(-)* also eliminated their neuroprotective effects (Fig. 2*B*), likely because the CsgA proteins produced by *csgB(-)* mutants can bind to CsgB produced by *csgA(-)* mutants. Such cross-seeding allows the assembly of curli fibril and was previously observed (19).

Next, we switched the diet of the PD animals between wild-type K12 and *csgA(-)* mutants at different developmental stages and found that the α-syn–induced locomotion defects and ADE degeneration are largely associated with post-stage 4 larva (L4) and adult consumption of the curli-producing bacteria (Fig. 2*C*). In contrast, the exposure to curli during larval development did not produce much effect on neurodegeneration. Since L4 and adult animals consumed more food than younger animals, the amount of curli uptake may be associated with the severity of the degenerative phenotypes.

Pharmacological Inhibition of *csgA* Expression Suppresses Neurodegeneration. In addition to genetic inactivation of curli subunits, we also used pharmacological agents to inhibit curli production and tested the effects on neurodegeneration. Epigallocatechin gallate (EGCG) is a polyphenol extracted from

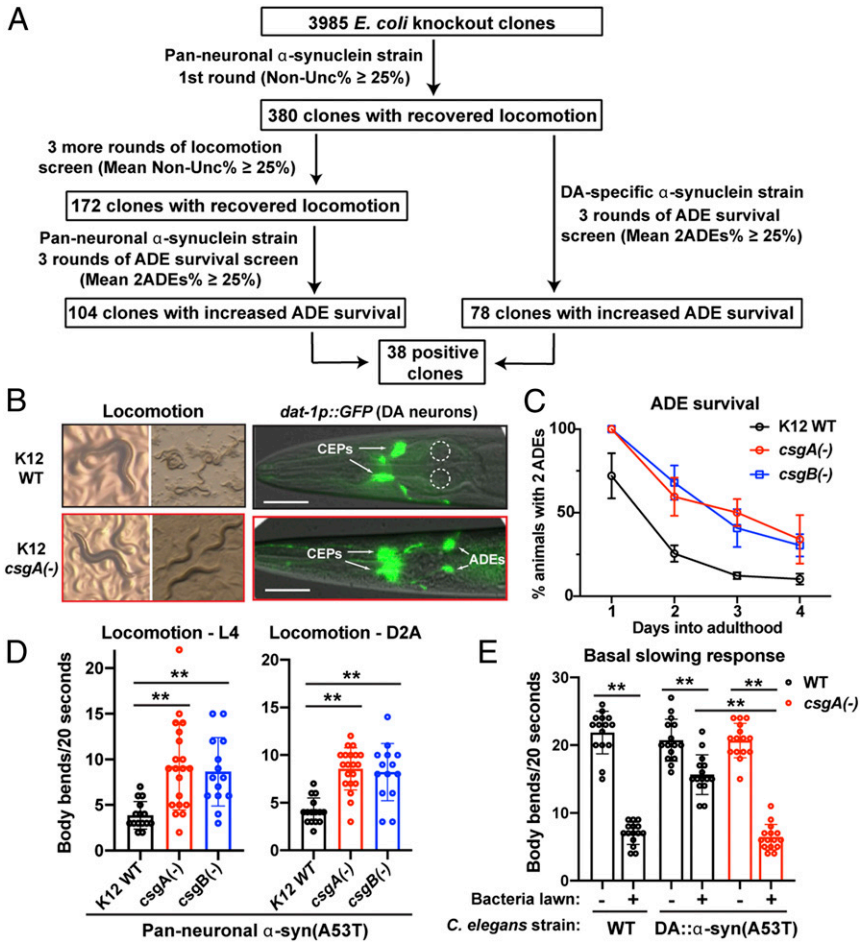

Fig. 1. Genome-wide screen for proneurodegenerative genes in *E. coli*. (*A*) A flowchart of the screen using UM10 *unkIs7[aex-3p::α-syn(A53T), dat-1p::gfp]* and UM6 *unkIs9 [dat-1p::α-syn(A53T), dat-1p::gfp]* strains and the Keio library. (*B*) Representative images of uncoordinated movement and ADE neurodegeneration in UM10 animals fed with wild-type (WT) K12 *E. coli* and the restored locomotion and intact ADE neurons in animals fed with *csgA*(-) K12. (*C*) Percentage of UM10 animals with two ADE neurons when fed with WT, *csgA*(-), and *csgB*(-) K12 on various days into adulthood. (*D*) Locomotion rate of UM10 animals at L4 stage and day-2-adult stage when fed with WT, *csgA*(-), and *csgB*(-) K12. Mean ± SD were shown, and each dot represents one animal assayed. (*E*) Locomotion rate of WT N2 and UM6 animals on and off the bacteria lawn. UM6 animals exhibited impairment in food-induced basal slowing response when fed with WT K12, and the slowing response was restored when UM6 animals were fed with *csgA(-)* K12. Double asterisks indicate statistical significance ($P < 0.01$) in multiple comparisons using ANOVA analysis followed by a Tukey's HSD post hoc test.

green tea and strongly inhibits biofilm formation by impairing curli assembly in *E. coli* (21). We confirmed that EGCG treatment completely eliminated the Congo red staining signal (Fig. 2*D*). To measure endogenous CsgA levels, we initially engineered the *csgA* locus to insert a carboxyl-terminal mCherry, but the resulted *csgA::mCherry* fusion completely blocked curli production (*SI Appendix*, Fig. S1*B*), suggesting that fusing large fluorescent proteins (~28 kDa for mCherry) with small amyloidogenic proteins (~15 kDa for CsgA) may interfere with fibril formation. We then inserted a small 3×FLAG tag at the *csgA* locus, and the resulted *K12-csgA::3×FLAG* strains produced normal levels of curli and formed biofilm as the wild-type K12. As expected, EGCG strongly inhibited endogenous *csgA* expression detected by the FLAG tag (Fig. 2*D*).

Because EGCG is also known to have neuroprotective effects in PD models (22), we set out to assess the contribution of its bacterial effects in neuroprotection. To our surprise, treating the K12 bacteria diet with EGCG alone is sufficient to create a strong inhibition of α-syn–induced neurodegeneration (Fig. 2*E*). The inhibitory effects were almost indistinguishable from the animals that also received the EGCG treatment in addition to being fed with the EGCG-treated diet. This result suggests that, at least in the *C. elegans* PD model, the neuroprotective effects of EGCG may be largely due to its activities in inhibiting bacterial curli production.

Bacterial Curli Promotes α-syn Aggregation. Because both CsgA and α-syn are rich in β-sheet structures, we next examined whether CsgA promotes α-syn aggregation in vivo. First, using a transgenic strain with muscle-specific expression of α-syn::YFP fusion, we found that the α-syn aggregation in the form of fluorescent puncta was strongly inhibited when the animals were fed with *csgA(-)* or *csgB(-)* bacteria (Fig. 3*A*). Conversely, when the animals were fed with a uropathogenic *E. coli* strain (UTI2) that has high levels of curli production (Fig. 2*A*), much more α-syn aggregates were observed than in animals grown on wild-type K12 (Fig. 3*A*). As expected, *csgA(-)* knockout in the UTI2 strain significantly reduced the number of aggregates. Thus, not only curli promotes α-syn aggregation but also the amount of curli consumed by the animals correlates with the severity of α-syn aggregation.

Because the α-syn::YFP fusion may not accurately reflect the aggregation pattern of α-syn, we next directly stained α-syn expressed pan-neuronally or specifically in DA neurons using anti–α-syn antibodies. We found that the number of α-syn proteins detected in *aex-3p::α-syn(A53T)* animals fed with *csgA(-)* bacteria was greatly reduced compared to the animals fed with wild-type K12 (Fig. 3*B*). In animals carrying the *dat-1p::α-syn(A53T)* transgene and fed with wild-type K12, α-syn proteins were found as discrete aggregates in both the cytoplasm and axons of DA neurons. Feeding with *csgA(-)* bacteria, however, removed most of the aggregates and led to a diffusive pattern of α-syn (Fig. 3*C*).

Biochemical analysis supported the immunofluorescence results. After sequentially fractionizing the lysate of animals expressing α-syn::YFP in the muscle, we found that the amount of α-syn::YFP was markedly reduced in the insoluble fraction in animals fed with *csgA(-)* K12 compared to the animals fed with wild-type K12 (Fig. 3*D*). In contrast, the α-syn::YFP level in the high-salt soluble (RAB) and detergent soluble (RIPA) fraction did not show much difference. In animals expressing α-syn(A53T) pan-neuronally, however, feeding with *csgA(-)* K12 led to the down-regulation of α-syn in the whole animal lysate and all three fractions (Fig. 3*D*).

Table 1. Deletion of 38 *E. coli* genes led to amelioration of α-syn–induced neurodegeneration

	Pan-neuronal α-syn (A53T)		DA-specific α-syn (A53T)	
Bacterial clones	Non-Unc%	2ADEs%	2ADEs%	Gene function
K12 WT	0%	6 ± 8%	11 ± 10%	
Curli amyloid fibril formation				
csgA(-)	33 ± 4%	50 ± 7%	50 ± 7%	Major subunit of curlin
csgB(-)	33 ± 8%	42 ± 6%	42 ± 12%	Minor subunit of curlin
LPS production and assembly				
lapA(-)	35 ± 9%	28 ± 8%	35 ± 19%	LPS assembly protein A
lapB(-)	41 ± 5%	35 ± 7%	42 ± 6%	LPS assembly protein B
lpcA(-)	35 ± 9%	42 ± 13%	33 ± 14%	Sedoheptulose 7-phosphate isomerase; LPS biosynthesis
rfe(-)	29 ± 16%	45 ± 15%	38 ± 8%	Synthesis of enterobacterial common antigen and LPS O-side chains
pldA(-)	28 ± 10%	43 ± 19%	30 ± 4%	Outer membrane phospholipase A; mlaA-dependent LPS hyperproduction
Adenosyl-cobalamin biosynthesis				
cobS(-)	31 ± 5%	35 ± 7%	33 ± 6%	Cobalamin 5′-phosphate synthase
btuR(-)	29 ± 4%	27 ± 6%	35 ± 11%	Cobinamide/cobalamin adenosyltransferase
eutT(-)	30 ± 5%	40 ± 15%	37 ± 10%	Putative ethanolamine utilization cobalamin adenosyltransferase
Inhibitors of eukaryotic lysozyme				
ivy(-)	45 ± 27%	43 ± 12%	42 ± 12%	Inhibitor of vertebrate lysozyme
ydhA(-)	30 ± 4%	43 ± 18%	32 ± 14%	Inhibitor of c-type lysozyme, putative lipoprotein
Oxidative stress response				
gpmI(-)	43 ± 17%	37 ± 10%	57 ± 17%	2,3-bisphosphoglycerate-independent phosphoglycerate mutase
yaaA(-)	43 ± 11%	45 ± 15%	28 ± 15%	Peroxide stress resistance protein
sodA(-)	35 ± 8%	38 ± 15%	30 ± 15%	Superoxide dismutase (Mn)
msrA(-)	38 ± 8%	38 ± 12%	30 ± 8%	Peptide methionine sulfoxide reductase
nrfA(-)	26 ± 10%	27 ± 2%	35 ± 11%	Cytochrome *c* nitrite reductase subunit
yfiD(-)	31 ± 5%	35 ± 7%	32 ± 2%	Stress-induced alternate pyruvate formate-lyase subunit
Metabolism and energy homeostasis				
pck(-)	39 ± 7%	37 ± 9%	48 ± 6%	Phosphoenolpyruvate carboxykinase; gluconeogenesis
tpiA(-)	26 ± 2%	27 ± 5%	43 ± 2%	Triose-phosphate isomerase; glycolysis and gluconeogenesis
ldhA(-)	39 ± 16%	25 ± 4%	27 ± 14%	D-lactate dehydrogenase
lldD(-)	29 ± 6%	31 ± 5%	30 ± 8%	L-lactate dehydrogenase
tdh(-)	31 ± 8%	32 ± 6%	32 ± 6%	Threonine dehydrogenase; major catabolic pathway for threonine utilization
cysQ(-)	41 ± 10%	38 ± 6%	28 ± 8%	3′(2′),5′-bisphosphate nucleotidase
nrdD(-)	26 ± 10%	38 ± 2%	27 ± 6%	Anaerobic ribonucleoside-triphosphate reductase; DNA synthesis
betA(-)	25 ± 13%	50 ± 16%	33 ± 12%	Choline dehydrogenase
Transporter				
yjcD(-)	31 ± 8%	33 ± 10%	38 ± 2%	Guanine/hypoxanthine transporter
mdtC(-)	30 ± 4%	43 ± 14%	37 ± 8%	Multidrug efflux pump RND permease subunit
ybbY(-)	29 ± 4%	40 ± 15%	32 ± 5%	Putative purine transporter
tolQ(-)	30 ± 6%	50 ± 11%	25 ± 12%	An inner membrane component of the Tol-Pal system
Transcription factors and DNA regulation				
yebC(-)	33 ± 7%	40 ± 16%	38 ± 6%	Putative transcriptional regulator
ybbS(-)	30 ± 6%	42 ± 16%	43 ± 2%	DNA-binding transcriptional activator
rdgC(-)	26 ± 5%	43 ± 15%	30 ± 14%	Nucleoid-associated protein RdgC
Others				
ppiD(-)	41 ± 17%	37 ± 16%	42 ± 10%	Periplasmic folding chaperone
baeS(-)	31 ± 4%	40 ± 8%	35 ± 21%	Sensory histidine kinase
ycaC(-)	31 ± 4%	38 ± 15%	42 ± 5%	Putative hydrolase
ybjQ(-)	30 ± 13%	32 ± 6%	43 ± 15%	Putative heavy metal binding protein
yfeY(-)	29 ± 2%	45 ± 15%	27 ± 17%	DUF1131 domain–containing lipoprotein

This down-regulation likely occurred at the protein level, because the α-syn messenger RNA (mRNA) level did not show any difference in animals fed with wild-type and *csgA(-)* K12 (*SI Appendix*, Fig. S2*A*), and treatment with proteasome inhibitors, such as MG132 and bortezomib, restored the protein level of α-syn in *aex-3p::α-syn(A53T)* animals fed with *csgA(-)* K12 (Fig. 3*E*). These data support the idea that CsgA derived from the bacteria promotes the formation of insoluble α-syn aggregates that are not accessible by the proteasomal machinery. Importantly, treatment with ubiquitination or proteasome inhibitors could largely block the neuroprotective effects of deleting *csgA* in the bacteria (Fig. 3*F*). Thus, in the absence of bacterial curli, neurons were capable of handling the proaggregating α-syn(A53T) proteins through the ubiquitination–proteasome system. Curli-induced α-syn aggregation may exacerbate the proteotoxic stress and overwhelm the proteasome system, leading to neurodegeneration.

CsgA Colocalizes with α-syn in Muscles and Neurons. We next tested whether bacteria curli can get into *C. elegans* tissues to promote α-syn aggregation through cross-seeding in vivo. According to the theory of cross-seeding (23), we hypothesized that CsgA serves as the seed to nucleate α-syn. Similar to the K12 strain, we engineered the

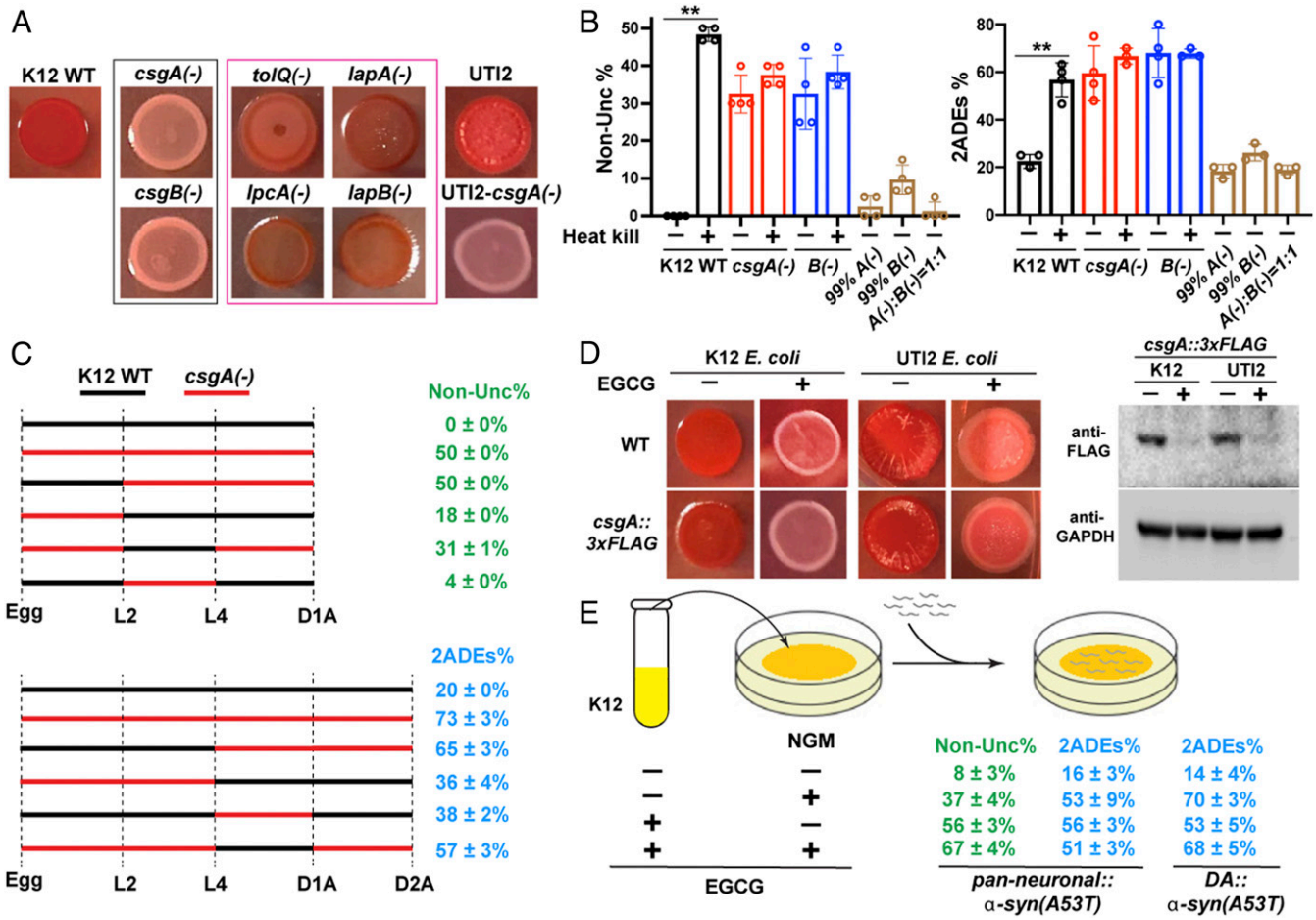

Fig. 2. Bacterial curli production promotes α-syn–induced neurodegeneration. (*A*) WT and mutant K12 *E. coli* and WT and *csgA(-)* UTI2 *E. coli* were grown on Congo red indicator plates at 25 °C for 2 d to visualize curli production. Curli subunit mutants are in the black box, and mutants that were found in our screen and also showed reduced curli production are in the pink box. (*B*) Percentage of UM10 *unkIs7[aex-3p::α-syn(A53T), dat-1p::gfp]* animals with non-Unc phenotype at L4 stage or with two ADE neurons at day-2-adult stage when fed with either heat-killed WT, *csgA*(-), and *csgB*(-) K12 or a mixture of WT with *csgA(-)* or *csgB(-)* K12 at 1:99 ratio [indicated as 99% A(-) or B(-), respectively] or a mixture of *csgA(-)* and *csgB(-)* at 1:1 ratio [indicated as A(-):B(-) = 1:1]. Mean ± SD were shown, and each dot represents one independent experiment with 20~30 animals scored. (*C*) Percentage of UM10 animals with non-Unc phenotype and two intact ADE neurons when fed with either K12 WT or *csgA(-)* at different developmental stages. The dotted lines indicate the timing of diet switch at specific stages from egg to day 1 adults (D1A) or day 2 adults (D2A). (*D*) WT K12 and UTI2 *E. coli* and their derivatives containing the *csgA::3×FLAG* genomic edits were grown on Congo red indicator plates with or without 200 μg/mL EGCG. Western blots of the bacteria lysate using anti-FLAG antibodies were used to confirm the inhibition of CsgA expression by EGCG. Anti-GAPDH blotting was used as a loading control. (*E*) Percentage of UM10 animals with non-Unc phenotype and two intact ADE neurons or the percentage of UM6 *unkIs9 [dat-1p::α-syn(A53T), dat-1p::gfp]* animals with two ADEs when grown on NGM plates that contained 200 μg/mL EGCG or empty vehicle and seeded with EGCG-treated or -untreated WT K12. For the treatment of K12 with EGCG, a single colony was cultured with LB medium containing 200 μg/mL EGCG overnight prior to seeding on NGM plate. The mean ± SD of three independent experiments (25 animals were scored for each experiment) is shown. Double asterisks indicate statistical significance ($P < 0.01$) in multiple comparisons using ANOVA analysis followed by a Tukey's HSD post hoc test.

csgA locus to fuse a carboxyl-terminal 3×FLAG tag in the UTI2 *E. coli* strain, which produced high levels of curli, and then fed this bacteria to animals expressing α-syn::YFP in the muscle. By staining the FLAG tag, we observed the colocalization of CsgA with α-syn::YFP puncta (Fig. 4*A*). Strikingly, CsgA appeared to be located in the center of the α-syn::YFP aggregates, which is consistent with the notion that curli helps nucleate α-syn. To avoid possible complication with the α-syn::YFP fusion, we directly visualize the colocalization of α-syn and CsgA through immunofluorescence double staining in animals expressing α-syn(A53T) in the muscle (Fig. 4*B*). In this case, the CsgA and α-syn signals appeared to overlap completely.

Colocalization of CsgA with α-syn was also observed in DA neurons of animals carrying the *dat-1p::α-syn(A53T)* transgene and fed with *UTI-2-csgA-3×FLAG* bacteria (Fig. 4*C*). Importantly, colocalization was not only found in the CEP and ADE neurons, which are adjacent to the pharynx that grinds up the bacteria, but also found in PDE neurons that are located in the posterior half of the body. Thus, the CsgA proteins appeared to be transported inside the *C. elegans* (Fig. 4*C*). Interestingly, CsgA signals were not observed in normal DA neurons that did not express α-syn, suggesting that the retention of bacterial curli also depends on α-syn aggregation (*SI Appendix*, Fig. S3). These results support the mutual cross-seeding between CsgA and α-syn.

As controls for the immunofluorescence double staining experiments, we fed PD animals with the wild-type UTI2 bacteria without the CsgA::3×FLAG fusion and did not observe any anti-FLAG signals (*SI Appendix*, Fig. S4). Deconvolution was used to analyze the antibody staining images to increase clarity and to remove out-of-focus light. The raw unprocessed images showed similar colocalization patterns (*SI Appendix*, Fig. S5).

Curli Promotes α-syn–Induced Mitochondrial Dysfunction and Energy Failure. We next conducted transcriptomics studies to investigate what molecular aspects of the α-syn neurodegenerative pathology

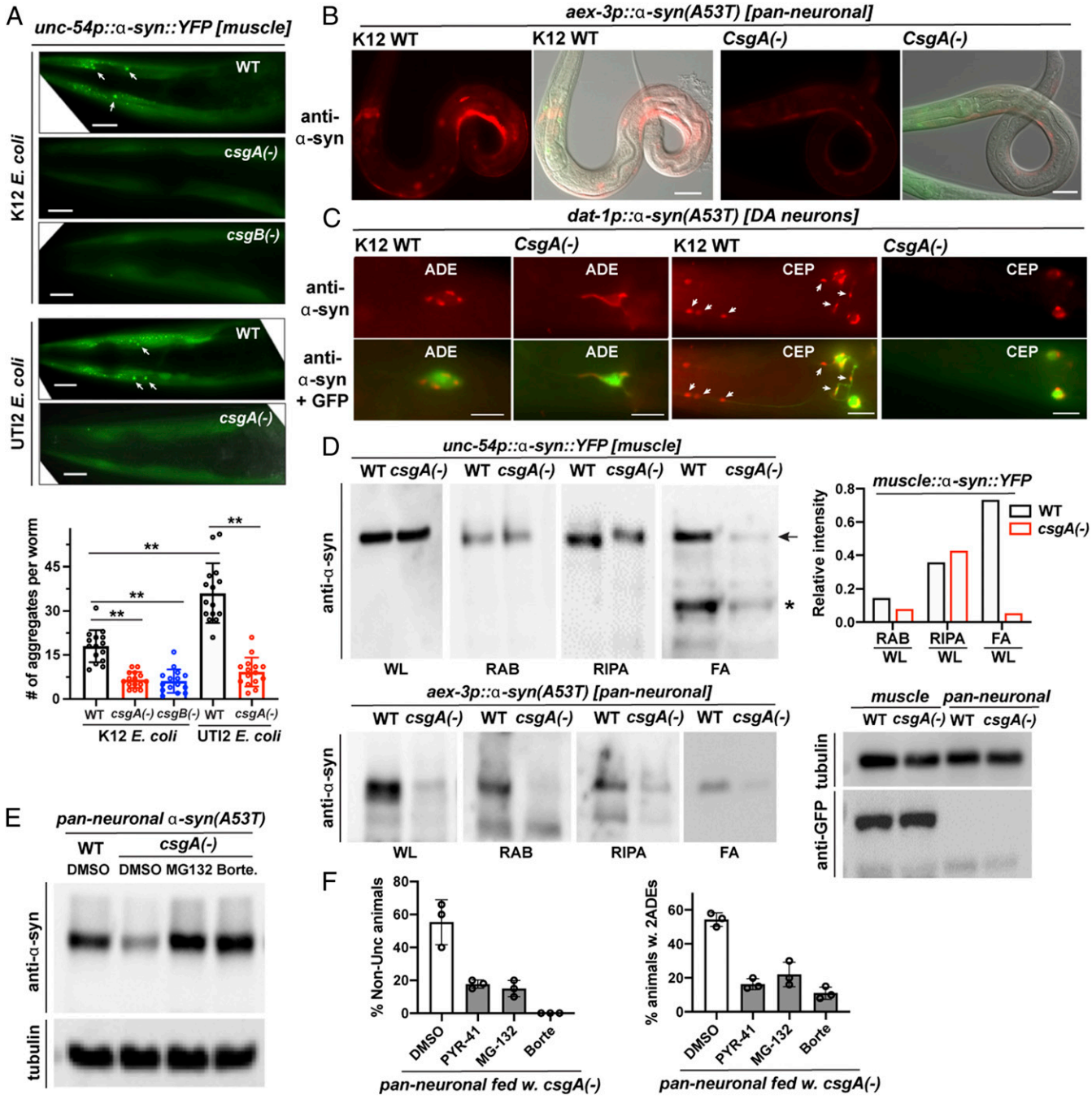

Fig. 3. Bacterial curli promotes α-syn aggregation. (*A*) Representative images of α-syn::YFP aggregates in the muscle of NL5901 *pkIs2386[unc-54p::α-syn::YFP; unc-119(+)]* animals fed with different bacteria. Aggregates at the head region of day-1 adults were shown. (Scale bar: 20 μm.) For image quantification, the number of fluorescent aggregates in the same head area were quantified for 15 worms per group. Mean ± SD were shown. (*B*) Anti–α-syn antibody staining of UM10 *unkIs7[aex-3p::α-syn(A53T), dat-1p::gfp]* animals at L2 stage fed with WT or *csgA*(-) K12. (Scale bar: 20 μm.) (*C*) Anti–α-syn staining showed the α-syn aggregates (arrows) in the DA neurons of day-2 adults in UM6 *unkIs9 [dat-1p::α-syn(A53T), dat-1p::gfp]* animals. Animals fed with *csgA*(-) K12 showed less aggregation. GFP expressed from the *dat-1* promoter labels the DA neurons. (Scale bar: 10 μm.) (*D*) Sequential fractionation of the lysate of NL5901 and UM10 animals fed with WT or *csgA*(-) K12 and different fractions were blotted by anti–α-syn antibodies in Western blot assays. Relative intensity of different fractions was quantified using ImageJ and normalized to whole animal lysate (WL). Anti-tubulin and anti-GFP blotting were used as internal controls. Arrow and asterisk indicate intact and degraded α-syn::YFP, respectively. (*E*) Western blot of α-syn and tubulin in the lysate of UM10 animals fed with WT K12 and treated with proteasome inhibitors MG132 (11 μM) and bortezomib (13 μM). (*F*) Percentage of UM10 animals with non-Unc phenotype and two intact ADE neurons under the treatment of ubiquitination inhibitor PYR-41 (1.4 mM) or proteasome inhibitors MG132 (11 μM) and bortezomib (13 μM). The mean ± SD of three independent experiments with 20~30 animals is shown. Double asterisks indicate statistical significance ($P < 0.01$) in multiple comparisons using ANOVA analysis followed by a Tukey's HSD post hoc test.

can be rescued by deleting CsgA in the bacteria. Through RNA sequencing (RNA-seq), we found 1,274 genes down-regulated (fold change > 2; adjusted $P < 0.05$) in animals expressing α-syn(A53T) pan-neuronally compared to wild-type animals when both fed with the wild-type K12. Gene ontology analysis found that genes that function in the mitochondria and genes that regulate metabolic

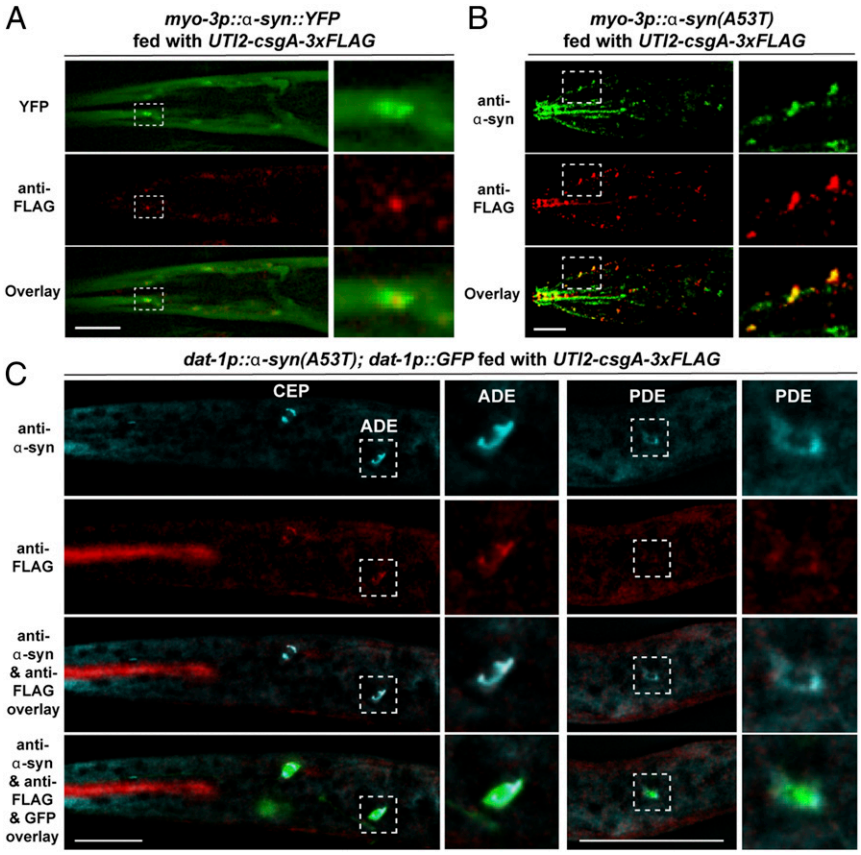

Fig. 4. *CsgA* colocalizes with α-syn. (*A*) Day-5 adults of NL5901 *pkIs2386[unc-54p::α-synuclein::YFP; unc-119(+)]* animals fed with *UTI2-csgA-3×FLAG* bacteria were stained with anti-FLAG (red) antibodies. *Insets* show the enlarged region outlined by the dashed box and indicate the colocalization of CsgA and α-syn. (*B*) Day-5 adults of CGZ512 *unkEx109[myo-3p::α-syn(A53T); dpy-5(+)]* animals fed with *UTI2-csgA-3×FLAG* bacteria were stained with anti–α-syn (green) and anti-FLAG (red) antibodies. Insets are enlarged images of the boxed regions. (*C*) Day-1 adults of UM6 *unkIs9[dat-1p::α-syn(A53T), dat-1p::gfp]* animals fed with *UTI2-csgA-3×FLAG* bacteria were stained with both anti–α-syn (cyan) and anti-FLAG (red) antibodies. GFP signal indicates the position of the DA neurons. Colocalization of CsgA and α-syn were observed in all three types of DA neurons, CEP, ADE, and PDE neurons. Inserts are enlarged images of the boxed regions showing the colocalization in ADE and PDE neurons. (Scale bars: 20 μm.) Images were processed using the Leica THUNDER imaging system. The raw images can be found in *SI Appendix*, Fig. S5.

processes and energy production were enriched in the 1,274 down-regulated genes, which indicated that α-syn aggregation disrupted mitochondrial functions. Among these 1,274 genes, 168 genes were up-regulated when *aex-3p::α-syn(A53T)* animals were fed with *csgA(-)* K12 bacteria (Fig. 5*A* and *SI Appendix*, Tables S1 and S2). Importantly, 84% (168/199) of the genes that were up-regulated by feeding with *csgA(-)* K12 were genes down-regulated by α-syn(A53T), and no significant transcriptomic changes were found between the wild-type animals fed with wild-type and *csgA(-)* K12 bacteria. Thus, promoting α-syn aggregation is likely the only activity of curli in the PD animals, and curli does not seem to affect other aspects of normal *C. elegans* physiology.

We next confirmed the down-regulation of seven mitochondrial genes (*alh-13*, *acdh-1*, *bcat-1*, *ech-6*, *hach-1*, *hpdh-1*, and *mel-32*) in PD animals and their restored expression upon feeding with *csgA(-)* bacteria using RT-qPCR (Fig. 5*B* and *SI Appendix*, Fig. S2*B*). Some of these genes regulate mitochondrial cellular respiration. For example, *acdh-1* (a short/branched-chain acyl-CoA dehydrogenase) and *ech-6* (a short chain enoyl-CoA hydratase) are involved in mitochondrial fatty acid β-oxidation, and *bcat-1* codes for a branched-chain amino acid (BCAA) aminotransferase that initiates the catabolism of BCAAs. Both β-oxidation and BCAA breakdown generate acetyl-CoA, which feeds into the tricarboxylic acid (TCA) cycle to produce NADH and $FADH_2$, which are then supplied for the electron transport chain to produce adenosine triphosphate (ATP) (24). *hpdh-1* (a hydroxyacid–oxoacid transhydrogenase) directly functions in the TCA cycle, and *mel-32* codes for a serine hydroxymethyltransferase, which is essential for maintaining mitochondrial respiration (25). Interestingly, knockdown of *bcat-1* was previously found to promote neurodegeneration in PD models (26). In addition, the expression of lipid elongases (*elo-5*, *elo-6*, and *elo-9*) and acyl-coA oxidase (*acox-2* and *F08A8.4*), which are known genetic modifiers of PD (27, 28), were down-regulated in *aex-3p::α-syn(A53T)* animals and recovered upon feeding with *csgA(-)* bacteria (*SI Appendix*, Tables S1 and S2).

Four (*acdh-1*, *ech-6*, *hach-1*, and *hpdh-1*) of the mitochondrial genes down-regulated in PD animals were also reported to function in a shunt pathway that detoxifies the branched-chain fatty acid propionate (29), suggesting that the accumulation of propionate may contribute to neurodegeneration. This idea is supported by the isolation of *E. coli* mutants [*cobS(-)*, *btuR(-)*, and *eutT(-)*] deficient in vitamin B12 synthesis in our screen, because the removal of B12 from the bacterial diet was known to activate the propionate shunt genes (12), thus countering the effects of α-syn aggregation.

To test whether the alteration in genetic programs associated with mitochondrial activities and metabolism led to defects in energy production, we measured oxygen consumption rates in *C. elegans* using the Agilent Seahorse XFe24 analyzer. We found that animals expressing α-syn(A53T) pan-neuronally had much lower basal and ATP-linked respiration than the wild-type animals. Feeding with *csgA(-)* bacteria strongly rescued cellular respiration (Fig. 5*C*). These results support that CsgA-induced α-syn aggregation caused mitochondrial dysfunction and energy failure, leading to neuronal cell death.

We also visualized mitochondrial morphology using a strain expressing *tomm-20::mcherry* fusion in the touch receptor neurons. When fed with wild-type K12, the expression of α-syn(A53T) led to fragmentation of the mitochondria, whereas feeding with *csgA(-)* K12 largely rescued the morphological defects of the mitochondria (Fig. 5*D*). A well-known mitochondrial response to proteotoxic stress is the activation of mitochondrial unfolded protein response (mitoUPR) pathways (30). In *C. elegans*, mitochondrial stress in neurons can trigger mitoUPR in intestine through intertissue signaling (31). As expected, we observed the activation of mitoUPR

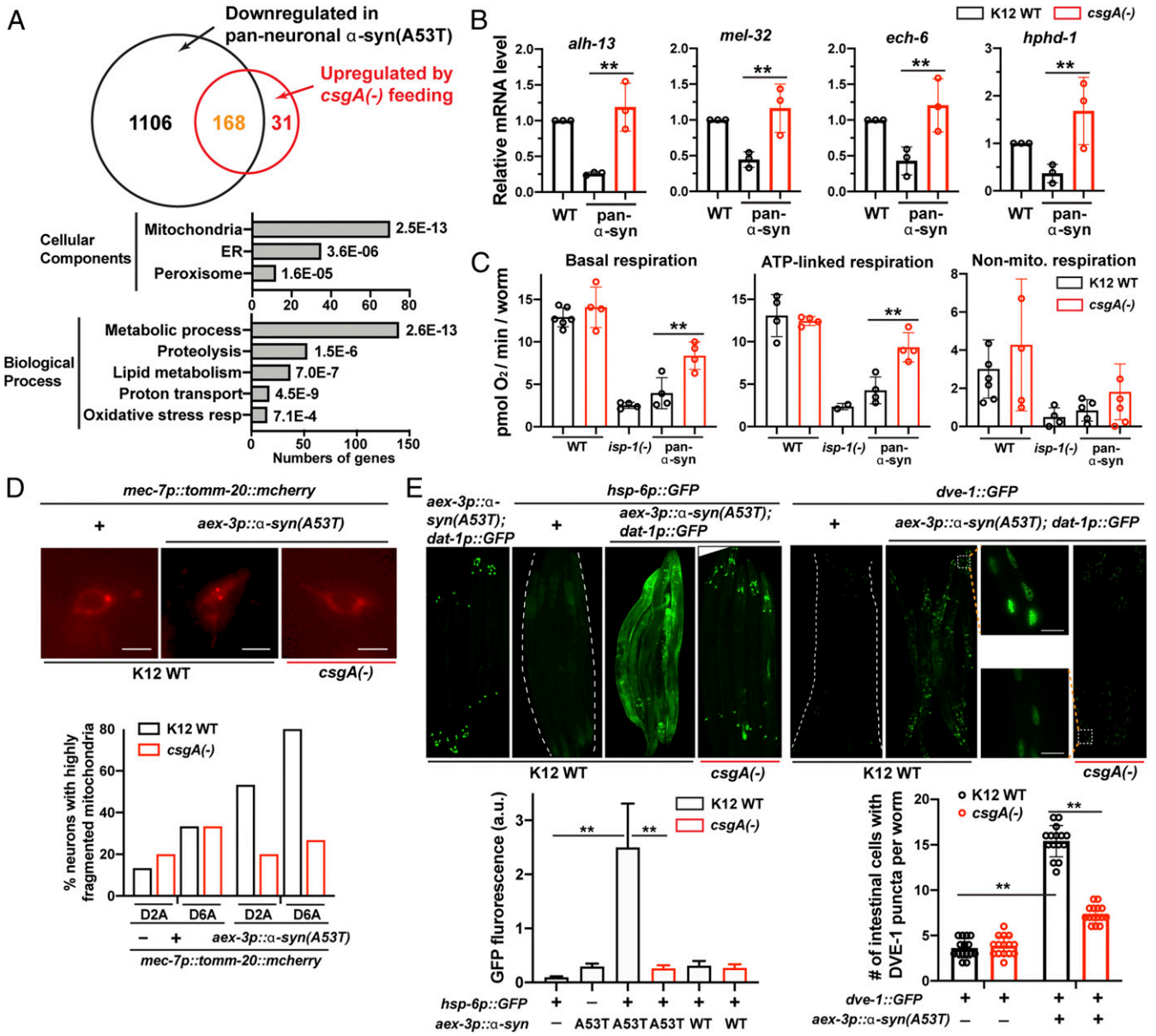

Fig. 5. Bacterial curli promotes α-syn–induced mitochondrial dysfunction. (*A*) Venn diagram of genes that are down-regulated in UM10 *unkIs7[aex-3p::α-syn(A53T), dat-1p::gfp]* animals compared to N2 control and genes that are up-regulated in UM10 animals fed with *csgA(-)* K12 compared to animals fed with WT K12. Gene ontology analysis for down-regulated genes between N2 and UM10 using the Database for Annotation, Visualization and Integrated Discovery (DAVID) tools. (*B*) RT-qPCR measurement of mRNA level of mitochondrial genes *alh-13*, *mel-32*, *ech-6*, and *hphd-1* in day-1 adults of UM10 animals fed with WT or *csgA(-)* K12 bacteria. Three biological replicates were performed, and mean ± SD were shown. (*C*) Basal respiration, ATP-linked respiration, and nonmitochondrial respiration (measured as oxygen consumption rate) of day-1 adults of N2, MQ887 *isp-1(qm150)*, and UM10 animals fed with WT or *csgA*(-) K12 bacteria. Representative results of 6~18 repeats for each condition were shown as mean ± SD. A total of 70 to 160 animals were added to each microplate well. (*D*) Representative images of the ALM neurons in CGZ833 *unkIs7; twnEx8[mec-7p::tomm-20::mCherry; myo-2p::GFP]* animals fed with WT or *csgA*(-) K12. (Scale bar: 2 μm.) Quantification shows the percentages of neurons with highly fragmented mitochondria in the soma in day-2 and day-6 adults. At least 20 animals were examined. (*E*) Representative images of *zcIs13[hsp-6::GFP]* and *zcIs39[dve-1p::GFP]* reporter expression in animals carrying *unkIs7[aex-3p::α-syn(A53T), dat-1p::gfp]* and fed with WT or *csgA*(-) K12 bacteria. Insets are enlarged images of the boxed region showing nuclear localization of DVE-1. (Scale bar: 25 μm.) Mean ± SD were shown for the quantification of the *hsp-6p::GFP* intensity and the number of intestinal cells showing DVE-1::GFP nuclear puncta (20 animals were analyzed for each experiment). Double asterisks indicate statistical significance ($P < 0.01$) in multiple comparisons using ANOVA analysis followed by a Tukey's HSD post hoc test.

markers *hsp-6::GFP* and *dve-1::GFP* in the intestine of animals with pan-neuronal expression of α-syn(A53T), and the mitoUPR response was not engaged when the animals were fed with *csgA(-)* bacteria (Fig. 5*E*). As controls, we found that the mitoUPR markers were not activated by the expression of wild-type α-syn, and the endoplasmic reticulum (ER) UPR marker *hsp-4::GFP* was not activated by either wild-type or A53T α-syn proteins (*SI Appendix*, Fig. S6). In fact, our transcriptomic analysis found that ER UPR genes (e.g., *hsp-3*, *apy-1*, and eight others) were enriched in genes down-regulated by α-syn(A53T) overexpression (*SI Appendix*, Table S1). Overall, our results indicate that bacterial curli is indispensable for the disruption of mitochondrial health by α-syn proteotoxicity.

Bacterial Curli Promotes Neurodegeneration Induced by Diverse Protein Aggregates in ALS, AD, and HD Models. In addition to α-syn in PD models, we also examined whether CsgA promoted the

neurodegeneration caused by other protein aggregates (e.g., SOD1 in ALS, amyloid β in AD, and huntingtin in HD. Using a *C. elegans* ALS model that expressed human SOD1(G85R)::YFP pan-neuronally (32), we found that, when the animals were fed with *csgA(-)* K12, the perinuclear accumulation of SOD1(G85R)::YFP aggregates largely disappeared in ALM neurons and the bright discrete puncta appeared more diffused and less aggregated in the ventral nerve cord motor neurons (Fig. 6*A*). Thus, CsgA may promote SOD1 aggregation.

For AD models, we employed two *C. elegans* strains that expressed Aβ1-42 either in a few pairs of sensory ASE neurons (using *flp-6* promoter) (33) or pan-neuronally (using *snb-1* promoter) (34). In the first model, we observed increased ASE neuron survival when the animals were fed with *csgA(-)* K12 instead of wild-type K12 (Fig. 6*B*). In the second case, we observed restored butanone associative learning upon the feeding with *csgA(-)* bacteria (Fig. 6*C*). Thus, eliminating bacteria curli could partially suppress A-β–induced neurodegeneration.

For HD models, we fed the animals expressing htt57-128Q::GFP fusion in the mechanosensory neurons (using *mec-3* promoter) with either wild-type or *csgA(-)* K12. The discrete perinuclear clusters of htt57-128Q::GFP signals became more diffused in animals fed with *csgA(-)* K12 and the degeneration of ALM neurons were also suppressed (Fig. 6*D*). As functional output, we tested harsh touch sensed by the PVD neurons and found that the percentage of response increased dramatically in the HD animals fed with *csgA(-)* K12, suggesting improved PVD functions (Fig. 6*E*). Nevertheless, we did not observe significant improvement in gentle touch response mediated by ALM and PLM neurons upon feeding with *csgA(-)* K12.

These results expanded the proneurodegenerative role of bacteria curli and suggested that CsgA may cross-seed not only α-syn but also a wide range of other aggregation-prone proteins, including SOD1, A-β, and polyQ-expanded huntingtin. Targeting CsgA may be generally effective in reducing neurodegeneration in many neurodegenerative diseases.

CsgA-Derived Amyloidogenic Peptides Cross-Seed α-syn and Induce Neuronal Death in Human Cells. Finally, we tested the in vivo cross-seeding of CsgA and α-syn in human neuroblastoma SH-SY5Y cells. After transfecting the SH-SY5Y cells with plasmids expressing α-syn wild-type or A53T, we treated the cells with a CsgA-derived amyloidogenic hexapeptide (N'-QYGGNN-C') or a nonamyloidogenic control (N'-QYGGNA-C') (35). We found that the CsgA amyloidogenic peptides significantly enhanced α-syn expression and aggregation in the SH-SY5Y cells (Fig. 7 *A* and *B*) and that the expression of α-syn or EGFP::α-syn fusion facilitated the accumulation of rhodamine-conjugated CsgA peptides (Fig. 7*C* and *SI Appendix*, Fig. S7*A*). In fact, without the expression of α-syn, the peptides cannot be retained in the SH-SY5Y cells. Thus, the cross-seeding and mutual facilitation of aggregation between CsgA and α-syn observed in *C. elegans* also occurred in human cells.

Using the rhodamine–QYGGNN peptide and antibody staining against α-syn, we directly observed the colocalization of CsgA-derived peptides with both α-syn wild-type and A53T proteins in SH-SY5Y cells (Fig. 7 *C* and *D* and *SI Appendix*, Fig. S7*B*). Both α-syn and CsgA appeared to be enriched in the periphery of the cells. α-syn(A53T) also showed a stronger staining signal than wild-type α-syn in the presence of CsgA peptides. To assess neuronal cell death, we carried out a cell viability assay on SH-SY5Y cells transfected with α-syn–expressing constructs and treated with the CsgA peptides. We found that the amyloidogenic QYGGNN, but not the control peptide, strongly exacerbated cell death induced by α-syn proteins (Fig. 7*E*). Treatment of the QYGGNN peptide alone in cells expressing no α-syn did not affect cell survival. Thus, bacterial curli may enhance the α-syn aggregate–induced degeneration of human neurons.

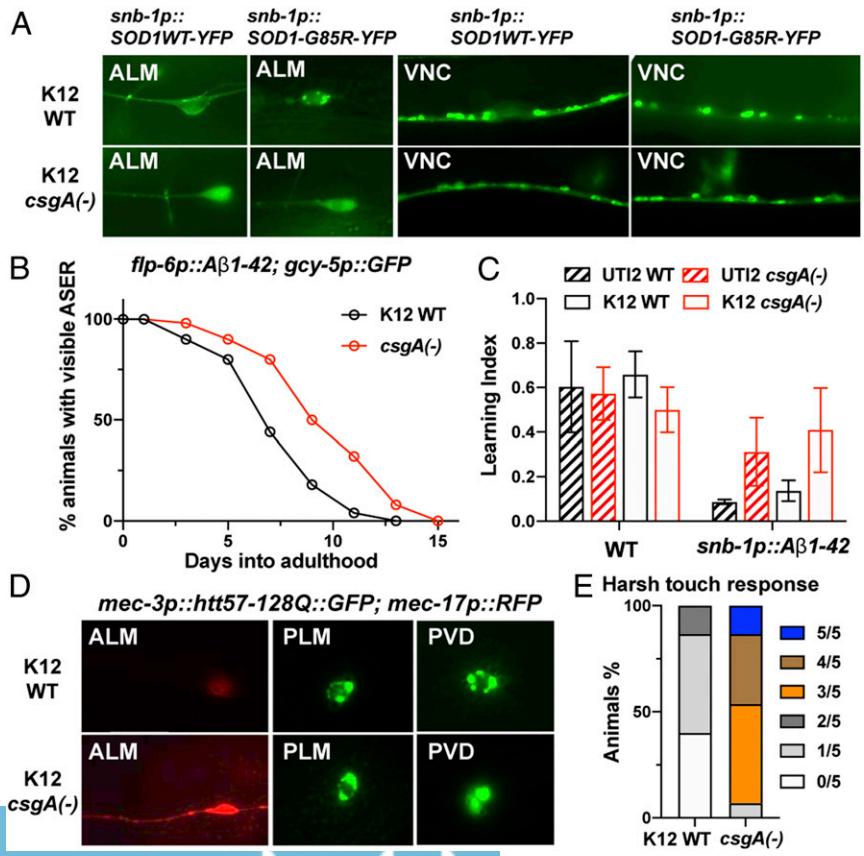

Fig. 6. Bacterial curli promotes neurodegeneration in *C. elegans* models of ALS, AD, and HD. (*A*) Representative images of ALM neurons and ventral nerve cord (VNC) neurons in ALS strains carrying the transgene *snb-1p::SOD1(G85R)::YFP* or *snb-1p::SOD1(WT)::YFP* and fed with WT or *csgA*(-) K12. At least 30 day-2 adults were assessed. (*B*) The percentage of animals with visible ASER neurons in FDX25 *sesIs25[flp-6p::Aβ1–42; gcy-5p::GFP; rol-6(D)]* animals fed with WT or *csgA*(-) K12. For each condition, 50 animals were scored. (*C*) Learning index of day-1 adults of CL2355 *smg-1(cc546) dvIs50 [snb-1p::Aβ1-42::3′UTR; mtl-2::GFP]* animals grown on WT and *csgA(-)* K12 and WT and *csgA(-)* UTI2 bacteria in an associative learning assay. A total of 2 to 400 animals were used in each experiment; three biological replicates and three technical replicates were performed. Mean ± SD is shown. (*D*) Morphological changes of the ALM neurons and the alteration of Huntingtin (Htt) aggregation pattern in PLM and PVD neurons in TU6295 *uIs115[mec-17p::TagRFP]; igIs5 [mec-3p::htt57-128Q::GFP; lin-15(+)]* animals fed with *csgA(-)* K12 compared to animals fed with WT K12. A total of 20 to 30 day-1 adults were assessed for each condition. (*E*) Harsh touch sensitivity of TU6295 animals fed with WT or *csgA*(-) K12 bacteria.

Discussion

Genome-Wide Screen Reveals Proneurodegenerative Factors in Bacteria. In this study, we conducted a genome-wide screen for proneurodegenerative factors in bacteria and identified 38 *E. coli* genes that promote α-syn–induced neurodegeneration in a *C. elegans* model of PD. The design of our screen ensured a low level of false positives, since two independent PD models were used and two independent phenotypes (locomotion defects and the loss of DA neurons) were scored (Fig. 1*A*). Nevertheless, we expected a relatively high false negative rate, since our screen strategy was biased toward the positive hits of the beginning rounds. Despite that, the final 38 positive *E. coli* genes clearly converged on several genetic pathways that likely play important roles in mediating bacteria–host interactions in PD pathogenesis. Besides the curli genes, *csgA* and *csgB*, which are the focus of this study, we also identified five genes involved in LPS production and assembly, three genes involved in the synthesis of adenosylcobalamin, two genes that code for inhibitors of eukaryotic lysozymes, six genes involved in oxidative stress response, and eight genes involved in metabolism and energy homeostasis, among others. These results not only confirmed some previous hypotheses about the gut microbiota–brain interactions in PD but also offered additional insights into the process.

For example, intact LPS triggers innate immunity in both *C. elegans* and humans, and the resulting neuroinflammatory response has detrimental effects on PD pathology (36, 37). Consistent with this notion, we observed that the disruption of LPS assembly in *E. coli* mutants, such as *lapA(-)* and *lapB(-)*, alleviated neurodegeneration in *C. elegans*. The receptor for LPS in *C. elegans* is, however, unclear, since the presumptive toll-like receptor signaling pathway does not mediate LPS toxicity (37). Thus, LPS may promote neurodegeneration through diverse molecular mechanisms in different organisms.

Deletions of *E. coli* genes (*cobS*, *btuR*, and *eutT*) involved in the synthesis of adenosylcobalamin, one active form of vitamin B12, also suppressed neurodegeneration in *C. elegans*. Since *E. coli* can only synthesize vitamin B12 through the salvage pathway, our results suggest that even the low amount of B12 in *E. coli* can have proneurodegenerative effects in the host. We hypothesize that vitamin B12 promotes degeneration by repressing genes that are also down-regulated by α-syn; these genes include components in the propionate breakdown shunt pathway (29). Although clinical studies suggested that vitamin B12 insufficiency may be a contributing factor for the cognitive impairment and rapid disease progression in PD (38), our results at the molecular level revealed that B12 may also be detrimental for PD in certain scenarios. Given that B12 is synthesized by gut bacteria in humans, the *C. elegans* model can be instrumental to understand the exact role of B12 in the microbial regulation of neuronal health.

Among the other positive hits, genes (e.g., *sodA*, *yaaA*, *msrA*, and *nrfA*) that help *E. coli* cope with oxidative stress, genes (*ldhA* and *lldD*) that mediate the conversion of lactate into pyruvate, and genes (*pck* and *tpiA*) that mediate key steps in gluconeogenesis also promoted α-syn–induced neurodegeneration. Although the mechanisms by which the above bacterial genes regulate host neurodegeneration await further investigation, our systematic screen successfully identified several possible routes of communication between the bacteria and host neurons.

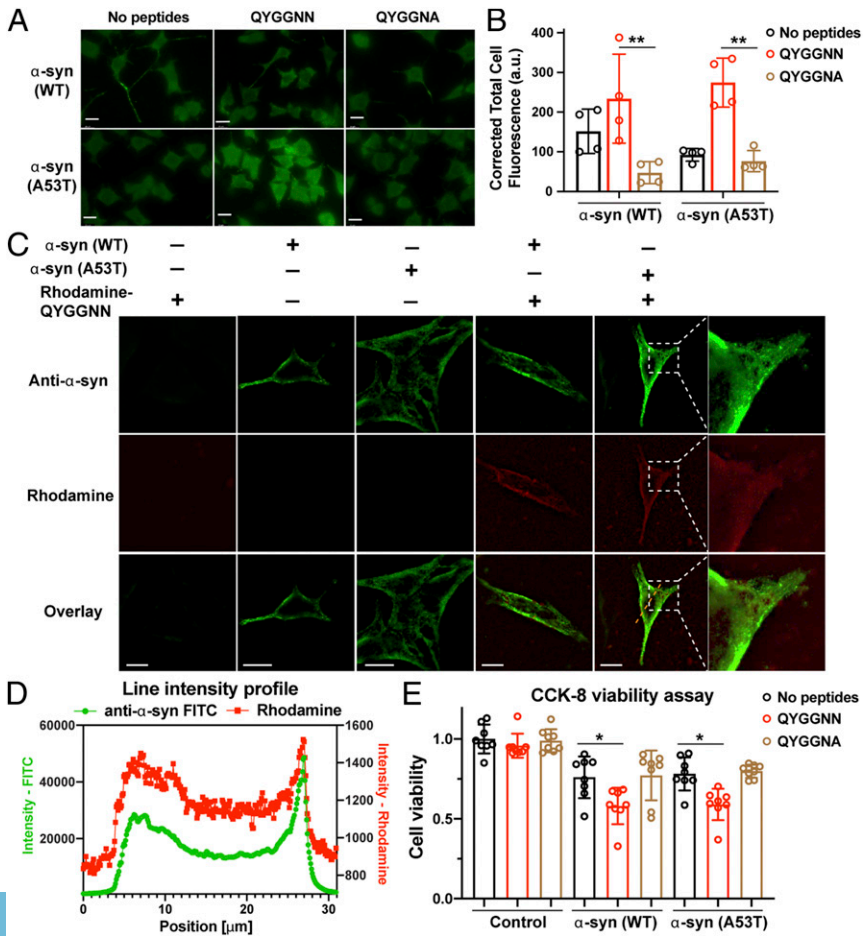

Fig. 7. *CsgA*-derived amyloidogenic peptides cross-seed α-syn and induce neuronal death in human cells. (*A*) Representative anti–α-syn immunofluorescent images of SH-SY5Y cells transfected with α-syn(WT or A53T)–expressing constructs and then treated with *CsgA*-derived amyloidogenic hexapeptides, nonamyloidogenic control, or empty vehicle. (Scale bars: 20 μm.) (*B*) Corrected total cell fluorescence (shown as mean ± SD) from the experiments shown in *A*. Amyloidogenic peptides significantly enhanced α-syn expression and accumulation in the SH-SY5Y cells. (*C*) SH-SY5Y cells transfected with α-syn(WT or A53T)–expressing constructs and treated with rhodamine-conjugated QYGGNN peptides (red) were then stained with anti–α-syn antibodies (green) to show colocalization of CsgA-derived peptides and α-syn. Insets are enlarged images of the boxed regions. Images were processed using the Leica THUNDER imaging system. The raw images can be found in *SI Appendix*, Fig. S7*B*. (*D*) Intensity profile for the orange dashed line in *C*. (*E*) Representative results of cell viability assays using α-syn(WT or A53T)–expressing SH-SY5Y cells treated with amyloidogenic hexapeptides, nonamyloidogenic control, or empty vehicle. Mean ± SD is shown, and the single asterisk indicates $P < 0.05$ in a one-way ANOVA followed by a Tukey's post hoc test.

Cross-Seeding between Bacteria Curli and Pathologically Aggregated Proteins in Neurons. Cross-seeding refers to the process by which oligomers composed by one type of misfolded proteins can promote the polymerization of another (23). Previous studies have observed the cross-seeding between A-β and other misfolded proteins, including prion, tau, and α-syn (39, 40). Bacterial curli, made of the major subunit CsgA and the minor subunit CsgB, is a type of amyloid fibril with cross β-sheet structure. Since curli fibers from different bacterial species are able to cross-seed in vitro and facilitate multispecies biofilm formation (41), it has been hypothesized that curli secreted by the gut bacteria may also cross-seed with A-β or α-syn and thus promote neurodegeneration (42). Direct evidence for this hypothesis was missing until recently.

While we were conducting this study, Sampson et al. (43) reported the in vitro cross-seeding between CsgA and α-syn and showed that purified CsgA accelerated α-syn fibrilization, which supported an earlier finding that curli enhanced α-syn deposition in the brain of aged rats (44). To extend these studies, we directly visualized the colocalization of CsgA and α-syn in vivo in *C. elegans* neurons and human neuroblastoma cells at the single-cell resolution. Importantly, previous studies mostly used Congo red staining to visualize bacteria curli, which may be problematic because Congo red stains not only curli but many other types of amyloid deposition (45). In this study, by tagging CsgA with a FLAG tag, we showed the presence of curli and their colocalization with α-syn inside neurons. Moreover, the cross-seeding is bidirectional. In both *C. elegans* neurons and human SH-SY5Y cells, CsgA promoted α-syn aggregation and α-syn facilitated the retention of CsgA. Similar bidirectional interaction was also observed between A-β and prions or α-syn (46).

In addition to the cross-seeding between curli and α-syn, we also showed that CsgA promoted neurodegeneration caused by the aggregation of A-β, SOD1, and polyQ-expanded huntingtin in *C. elegans* models of AD, ALS, and HD, respectively. Therefore, the bacteria-secreted curli may have detrimental effects in a range of neurodegenerative disorders. Targeting curli production in the gut may represent a general therapeutic approach to prevent or slow down the progression of protein aggregation diseases. In this study, we showed that blocking curli production in bacteria using EGCG, a green tea extract, had remarkable effects in preventing neurodegeneration, suggesting that pharmacological inhibition of curli may be an effective treatment for PD and likely other neurodegenerative diseases. In a recent study using a mouse PD model, Sampson et al. (43) found that colonization of mouse gut with curli-producing *E. coli* also promoted α-syn pathology in the brain and exacerbated motor impairment. Thus, the effects of curli on neurodegeneration appeared to be consistent across different disease models in diverse organisms.

Bacteria–Host Interactions Regulate Neuronal Mitochondrial Functions. Mitochondrial dysfunction is a hallmark of PD pathogenesis, and α-syn aggregation and mitochondrial damage exacerbate each other through a vicious cycle (2). Consistent with this idea, our transcriptomic studies found that α-syn(A53T) overexpression down-regulated genes that function in mitochondria, lipid metabolism, and ATP production. Eliminating bacterial curli restored the expression of a subset of these genes (e.g., mitochondrial genes *acdh-1*, *bcat-1*, *ech-6*, and *hpdh-1*), which may be the key regulatory points in the metabolic network disrupted in PD. This correction in the transcriptional program is accompanied by restored mitochondrial morphology, blocked mitoUPR activation, and revived cellular respiration. Thus, removing curli from the bacteria may prevent neuronal death by rescuing mitochondrial dysfunction and energy failure.

Supporting the above ideas, *bcat-1* was recently identified as a PD-associated gene (26). Human BCAT-1 is highly expressed in the substantia nigra of healthy individuals, but its expression is significantly diminished in PD patients. Knockdown of *bcat-1* in *C. elegans* neurons recapitulated aging phenotypes and enhanced α-syn–induced neurodegeneration. Since BCAT-1 is the aminotransferase that catalyzes the initial step of BCAA breakdown, down-regulation of *bcat-1* leads to not only reduced energy production but also increased BCAA levels, which appeared to correlate with disease severity in PD patients (47). In another example, impaired fatty acid β-oxidation is associated with the energy crisis in PD, and the levels of short chain 3-hydroxyacyl-CoA dehydrogenase (SCHAD), a key enzyme in β-oxidation, are significantly reduced in the ventral midbrain of both PD mice and PD patients (48). Overexpression of SCHAD mitigates the impairment of oxidative phosphorylation and ATP production in PD models (49). Our work found that *acdh-1* (a short/branched-chain acyl-CoA dehydrogenase, homolog of human ACADSB) and *ech-6* (a short chain enoyl-CoA hydratase, homolog of human ECHS1), two other essential enzymes in β-oxidation, were also down-regulated in PD but recovered after eliminating bacteria curli. Restoration of the expression of these key metabolic genes may be critical for restoring mitochondrial respiration and energy production at the cellular level.

Materials and Methods

***C. elegans* Strains.** *C. elegans* wild-type (N2) and mutant strains were maintained at 20 °C as previously described (50). PD-related strains UM9 *unkIs11 [dat-1p::GFP]*, UM10 *unkIs7[aex-3p::α-syn(A53T), dat-1p::gfp]*, UM11 *unkIs8[aex-3p::α-syn(WT), dat-1p::gfp]*, UM3 *unkIs10 [dat-1p::α-syn(WT), dat-1p::gfp]*, and UM6 *unkIs9 [dat-1p::α-syn(A53T), dat-1p::gfp]* were generous gifts from Garry Wong, Faculty of Health Sciences, University of Macau, Macau, China. ALS strains carrying the transgenes *snb-1p::SOD1(G85R)::YFP]* and *snb-1p::SOD1(WT)::YFP* were kindly provided by Jiou Wang, Bloomberg School of Public Health, Johns Hopkins University, Baltimore, MD. The AD strains carrying *sesIs25 [flp-6p::Abeta1-42; gcy-5p::GFP;rol-6]* were kindly provided by Monica Driscoll, Department of Molecular Biology and Biochemistry, Rutgers University, New Brunswick, NJ. CGZ512 *dpy-5(e907); unkEx109[myo-3p::α-syn(A53T); dpy-5(+)]* were generated in this study through microinjections. The *myo-3p::α-syn(A53T)* constructs were created by swapping the *dat-1* promoter in the *dat-1p::α-syn(A53T)* construct provided by Garry Wong with a 2.5-kb *myo-3* promoter.

Another PD strain, NL5901 *pkIs2386[unc-54p::α-synuclein::YFP; unc-119(+)]* the AD strain CL2355 *smg-1(cc546); dvIs50[pCL45 (snb-1::Aβ1-42::3′UTR(long); mtl-2:: GFP]*, the HD strain ID5 *igIs5 [mec-3p::htt57-128Q::GFP; lin-15(+)]*, the mitochondrial marker CLP215 *twnEx8[mec-7p::tomm-20::mCherry; myo-2p::GFP]*, and the mitoUPR reporters SJ4100 *zcIs13[hsp-6::GFP]* and SJ4197 *zcIs39[dve-1p::dve-1::GFP]* were provided by the Caenorhabditis Genetics Center.

Keio Library Screens. The Keio library (18) was purchased from Dharmacon. *E. coli* knockout clones from the library were grown overnight at 37 °C in lysogeny broth medium with 50 μg/mL kanamycin in 96-deep-well plates. A total of 20 μL overnight culture was seeded onto nematode growth medium (NGM) agar-containing 96-well plates. For locomotion screens, about 20 synchronized L1 animals of the UM10 strain were added into each well, and the animals were grown for 48 h at 20 °C before scoring for the penetrance of the non-Unc phenotype at the L4 stage. *E. coli* mutants that caused at least 25% of the animals in the well to be non-Unc were considered positive hits. Animals fed with the parental K12 (BW25113) served as the negative control. We refer to BW25113 as the wild-type K12 strain in this study. For the ADE survival screen, bacterial culture was seeded on a 5-cm Petri dish containing NGM and about 20 L1 animals of either UM10 or UM6 strains were added to the plate. Animals were screened as day-2 adults for the percentage of animals showing two ADE neurons that clearly expressed GFP and showed normal cell morphology.

Other Assays. Detailed information about all of the other assays we performed (*E. coli* genetic engineering, Congo red staining, Western blot, RNA-seq and RT-qPCR, antibody staining and fluorescent imaging, human cell culture, transfection, immunostaining, cell viability assay, *C. elegans* basal slowing response assays, butanone associative learning assays, and mitochondrial respiration assay) can be found in *SI Appendix*.

Statistical Analysis. All quantitative data were shown as mean ± SD. For statistical analysis, we used a one-way ANOVA followed by a Tukey's honestly significant difference (HSD) post hoc test to compare different treatments in a multiple comparison. A two-tailed Student's *t* test was used to compare two

groups. Differences were considered significant at $P < 0.05$. Double asterisks in figures indicate $P < 0.01$. All statistical analysis was carried out using GraphPad Prism 8.0 software (GraphPad Software).

Data Availability. The raw Western blot data (related to Figs. 2*D* and 3 *D* and *E*) can be accessed through https://doi.org/10.17632/vyc23scp8p.1 in Mendeley Data. The raw RNA-seq data can be accessed through https://www.ncbi.nlm.nih.gov/geo/query/acc.cgi?acc=GSE169204 in the Gene Expression Omnibus database.

ACKNOWLEDGMENTS. We thank Tingying Xia and Aixin Yan (School of Biological Sciences, The University of Hong Kong) and Patrick C. Y. Woo (Department of Microbiology, Li Ka Shing Faculty of Medicine, The University of Hong Kong) for providing the *E. coli* UTI2 strain, which was isolated at Queen Mary Hospital, Hong Kong. We thank Garry Wong, Jiou Wang, and Monica Driscoll for sharing strains. We also thank Aixin Yan, Jetty Lee, and Xiang Li at the University of Hong Kong for sharing equipment and reagents. Some strains used in this study were provided by the Caenorhabditis Genetics Center, which is funded by the NIH Office of Research Infrastructure Programs (P40 OD010440). This work was supported by grants from the Food and Health Bureau of Hong Kong (Health and Medical Research Fund Grant 07183186 to C.Z.), the Research Grants Council of Hong Kong (Early Career Scheme Grant 27104219 and Collaborative Research Fund Grant C7026-20G to C.Z.), and the University of Hong Kong (Seed Fund 201910159087 to C.Z.).

1. P. M. Douglas, A. Dillin, Protein homeostasis and aging in neurodegeneration. *J. Cell Biol.* **190**, 719–729 (2010).
2. W. Poewe *et al.*, Parkinson disease. *Nat. Rev. Dis. Primers* **3**, 17013 (2017).
3. L. Stefanis, α-Synuclein in Parkinson's disease. *Cold Spring Harb. Perspect. Med.* **2**, a009399 (2012).
4. E. M. M. Quigley, Microbiota-brain-gut axis and neurodegenerative diseases. *Curr. Neurol. Neurosci. Rep.* **17**, 94 (2017).
5. T. R. Sampson *et al.*, Gut microbiota regulate motor deficits and neuroinflammation in a model of Parkinson's disease. *Cell* **167**, 1469–1480.e12 (2016).
6. E. M. Quigley, Gastrointestinal dysfunction in Parkinson's disease. *Semin. Neurol.* **16**, 245–250 (1996).
7. A. H. Tan *et al.*, Helicobacter pylori infection is associated with worse severity of Parkinson's disease. *Parkinsonism Relat. Disord.* **21**, 221–225 (2015).
8. M. Barichella *et al.*, Unraveling gut microbiota in Parkinson's disease and atypical parkinsonism. *Mov. Disord.* **34**, 396–405 (2019).
9. F. Hopfner *et al.*, Gut microbiota in Parkinson disease in a northern German cohort. *Brain Res.* **1667**, 41–45 (2017).
10. T. Harach *et al.*, Reduction of Abeta amyloid pathology in APPPS1 transgenic mice in the absence of gut microbiota. *Sci. Rep.* **7**, 41802 (2017).
11. A. Cattaneo *et al.*, Association of brain amyloidosis with pro-inflammatory gut bacterial taxa and peripheral inflammation markers in cognitively impaired elderly. *Neurobiol. Aging* **49**, 60–68 (2017).
12. E. Watson *et al.*, Interspecies systems biology uncovers metabolites affecting *C. elegans* gene expression and life history traits. *Cell* **156**, 759–770 (2014).
13. J. Zhang *et al.*, A delicate balance between bacterial iron and reactive oxygen species supports optimal *C. elegans* development. *Cell Host Microbe* **26**, 400–411.e3 (2019).
14. A. Ray, B. A. Martinez, L. A. Berkowitz, G. A. Caldwell, K. A. Caldwell, Mitochondrial dysfunction, oxidative stress, and neurodegeneration elicited by a bacterial metabolite in a *C. elegans* Parkinson's model. *Cell Death Dis.* **5**, e984 (2014).
15. A. Urrutia *et al.*, Bacterially produced metabolites protect *C. elegans* neurons from degeneration. *PLoS Biol.* **18**, e3000638 (2020).
16. M. E. Goya *et al.*, Probiotic *Bacillus subtilis* protects against α-synuclein aggregation in *C. elegans*. *Cell Rep.* **30**, 367–380.e7 (2020).
17. M. Lakso *et al.*, Dopaminergic neuronal loss and motor deficits in *Caenorhabditis elegans* overexpressing human alpha-synuclein. *J. Neurochem.* **86**, 165–172 (2003).
18. T. Baba *et al.*, Construction of *Escherichia coli* K-12 in-frame, single-gene knockout mutants: The Keio collection. *Mol Syst Biol* **2**, 2006.0008 (2006).
19. M. L. Evans, M. R. Chapman, Curli biogenesis: Order out of disorder. *Biochim. Biophys. Acta* **1843**, 1551–1558 (2014).
20. D. R. Smith *et al.*, The production of curli amyloid fibers is deeply integrated into the biology of *Escherichia coli*. *Biomolecules* **7**, 75 (2017).
21. D. O. Serra, F. Mika, A. M. Richter, R. Hengge, The green tea polyphenol EGCG inhibits *E. coli* biofilm formation by impairing amyloid curli fibre assembly and downregulating the biofilm regulator CsgD via the σ(E) -dependent sRNA RybB. *Mol. Microbiol.* **101**, 136–151 (2016).
22. Y. Xu *et al.*, Epigallocatechin gallate (EGCG) inhibits alpha-synuclein aggregation: A potential agent for Parkinson's disease. *Neurochem. Res.* **41**, 2788–2796 (2016).
23. R. Morales, I. Moreno-Gonzalez, C. Soto, Cross-seeding of misfolded proteins: Implications for etiology and pathogenesis of protein misfolding diseases. *PLoS Pathog.* **9**, e1003537 (2013).
24. D. Nolfi-Donegan, A. Braganza, S. Shiva, Mitochondrial electron transport chain: Oxidative phosphorylation, oxidant production, and methods of measurement. *Redox Biol.* **37**, 101674 (2020).
25. S. Lucas, G. Chen, S. Aras, J. Wang, Serine catabolism is essential to maintain mitochondrial respiration in mammalian cells. *Life Sci. Alliance* **1**, e201800036 (2018).
26. V. Yao *et al.*, An integrative tissue-network approach to identify and test human disease genes. *Nat. Biotechnol.* 10.1038/nbt.4246. (2018).
27. Y. J. Lee, S. Wang, S. R. Slone, T. A. Yacoubian, S. N. Witt, Defects in very long chain fatty acid synthesis enhance alpha-synuclein toxicity in a yeast model of Parkinson's disease. *PLoS One* **6**, e15946 (2011).
28. X. Chen, R. D. Burgoyne, Identification of common genetic modifiers of neurodegenerative diseases from an integrative analysis of diverse genetic screens in model organisms. *BMC Genomics* **13**, 71 (2012).
29. E. Watson *et al.*, Metabolic network rewiring of propionate flux compensates vitamin B12 deficiency in *C. elegans*. *eLife* **5**, e17670 (2016).
30. N. S. Anderson, C. M. Haynes, Folding the mitochondrial UPR into the integrated stress response. *Trends Cell Biol.* **30**, 428–439 (2020).
31. Q. Zhang *et al.*, The mitochondrial unfolded protein response is mediated cell-non-autonomously by retromer-dependent Wnt signaling. *Cell* **174**, 870–883.e17 (2018).
32. J. Wang *et al.*, An ALS-linked mutant SOD1 produces a locomotor defect associated with aggregation and synaptic dysfunction when expressed in neurons of *Caenorhabditis elegans*. *PLoS Genet.* **5**, e1000350 (2009).
33. I. Melentijevic *et al.*, *C. elegans* neurons jettison protein aggregates and mitochondria under neurotoxic stress. *Nature* **542**, 367–371 (2017).
34. Y. Wu *et al.*, Amyloid-beta-induced pathological behaviors are suppressed by *Ginkgo biloba* extract EGb 761 and ginkgolides in transgenic *Caenorhabditis elegans*. *J. Neurosci.* **26**, 13102–13113 (2006).
35. C. Tükel *et al.*, Responses to amyloids of microbial and host origin are mediated through toll-like receptor 2. *Cell Host Microbe* **6**, 45–53 (2009).
36. L. P. Kelly *et al.*, Progression of intestinal permeability changes and alpha-synuclein expression in a mouse model of Parkinson's disease. *Mov. Disord.* **29**, 999–1009 (2014).
37. A. Aballay, E. Drenkard, L. R. Hilbun, F. M. Ausubel, *Caenorhabditis elegans* innate immune response triggered by *Salmonella enterica* requires intact LPS and is mediated by a MAPK signaling pathway. *Curr. Biol.* **13**, 47–52 (2003).
38. S. J. McCarter *et al.*, Low vitamin B12 and Parkinson disease: Potential link to reduced cholinergic transmission and severity of disease. *Mayo Clin. Proc.* **94**, 757–762 (2019).
39. R. Morales *et al.*, Molecular cross talk between misfolded proteins in animal models of Alzheimer's and prion diseases. *J. Neurosci.* **30**, 4528–4535 (2010).
40. P. K. Mandal, J. W. Pettegrew, E. Masliah, R. L. Hamilton, R. Mandal, Interaction between Abeta peptide and alpha synuclein: Molecular mechanisms in overlapping pathology of Alzheimer's and Parkinson's in dementia with Lewy body disease. *Neurochem. Res.* **31**, 1153–1162 (2006).
41. Y. Zhou *et al.*, Promiscuous cross-seeding between bacterial amyloids promotes interspecies biofilms. *J. Biol. Chem.* **287**, 35092–35103 (2012).
42. R. P. Friedland, Mechanisms of molecular mimicry involving the microbiota in neurodegeneration. *J. Alzheimers Dis.* **45**, 349–362 (2015).
43. T. R. Sampson *et al.*, A gut bacterial amyloid promotes α-synuclein aggregation and motor impairment in mice. *eLife* **9**, e53111 (2020).
44. S. G. Chen *et al.*, Exposure to the functional bacterial amyloid protein curli enhances alpha-synuclein aggregation in aged fischer 344 rats and *Caenorhabditis elegans*. *Sci. Rep.* **6**, 34477 (2016).
45. C. Y. Ho, J. C. Troncoso, D. Knox, W. Stark, C. G. Eberhart, Beta-amyloid, phospho-tau and alpha-synuclein deposits similar to those in the brain are not identified in the eyes of Alzheimer's and Parkinson's disease patients. *Brain Pathol.* **24**, 25–32 (2014).
46. R. Morales, K. M. Green, C. Soto, Cross currents in protein misfolding disorders: Interactions and therapy. *CNS Neurol. Disord. Drug Targets* **8**, 363–371 (2009).
47. H. Luan *et al.*, Comprehensive urinary metabolomic profiling and identification of potential noninvasive marker for idiopathic Parkinson's disease. *Sci. Rep.* **5**, 13888 (2015).
48. S. Przedborski, K. Tieu, C. Perier, M. Vila, MPTP as a mitochondrial neurotoxic model of Parkinson's disease. *J. Bioenerg. Biomembr.* **36**, 375–379 (2004).
49. K. Tieu *et al.*, L-3-hydroxyacyl-CoA dehydrogenase II protects in a model of Parkinson's disease. *Ann. Neurol.* **56**, 51–60 (2004).
50. S. Brenner, The genetics of *Caenorhabditis elegans*. *Genetics* **77**, 71–94 (1974).